Idiosyncratic and systematic aspects of spatial representations in the macaque parietal cortex

Steve W. C. Chang[1,2] and Lawrence H. Snyder

Department of Anatomy and Neurobiology, Washington University School of Medicine, St. Louis, MO 63110

Edited by Thomas D. Albright, The Salk Institute for Biological Studies, La Jolla, CA, and approved March 9, 2010 (received for review November 15, 2009)

The sensorimotor transformations for visually guided reaching were originally thought to take place in a series of discrete transitions from one systematic frame of reference to the next with neurons coding location relative to the fixation position (gaze-centered) in occipital and posterior parietal areas, relative to the shoulder in dorsal premotor cortex, and in muscle- or joint-based coordinates in motor output neurons. Recent empirical and theoretical work has suggested that spatial encodings that use a range of idiosyncratic representations may increase computational power and flexibility. We now show that neurons in the parietal reach region use nonuniform and idiosyncratic frames of reference. We also show that these nonsystematic reference frames coexist with a systematic compound gain field that modulates activity proportional to the distance between the eyes and the hand. Thus, systematic and idiosyncratic signals may coexist within individual neurons.

gain field | posterior parietal cortex | reference frame transformation

We are currently at a theoretical crossroads regarding how the brain computes motor commands from sensory information. The linear systems engineering tradition taught that neural circuits are assembled to compute particular transfer functions and that intermediate stages represent quantities with straightforward physical interpretations (1). At each stage, neurons encode information in a single frame of reference, which facilitates simple pooling. Each cell has a unique receptive field or preferred direction. This results in a distributed population code where each neuron encodes similar information in a similar manner. The vestibular–ocular reflex provides an example of this approach. Head rotation, measured by the vestibular semicircular canals using a canal-centered frame of reference, was believed to be transformed directly into oculomotor commands by virtue of appropriate synaptic weights on vestibular and oculomotor nuclei neurons (1). Visually guided reaching provides another example. Visual spatial information was originally thought to undergo a series of discrete transformations from a sensory (gaze-centered) frame of reference in the occipital and parietal cortices to hand-centered in the premotor cortex (extrinsic motor coordinates) and finally, to muscle commands in the primary motor cortex (intrinsic motor commands) (2–6). The parietal reach region (PRR) in the posterior parietal cortex (PPC) was seen as a discrete processing stage in which reach-related spatial information was encoded using a uniform gaze-centered reference frame and passed on to dorsal premotor cortex (PMd) (7, 8).

An alternative design borrows from connectionist principles and the field of artificial intelligence. In a trained neural network, the organizational principles may be obscure and individual nodes may encode information idiosyncratically (9, 10). Flexibility and computational power are increased when individual nodes code diverse, seemingly random permutations of the input. Subsequent processing can pick and choose from these diverse representations to perform arbitrarily complex operations on the inputs (11–17). Consistent with these ideas, recent work has revealed brain areas in which neurons use multiple complex reference frames. For example, cells in the superior colliculus code auditory stimuli using complex representations that are idiosyncratic to individual cells and neither purely gaze- nor purely head-centered (18, 19). Similar complex and nonuniform coding may occur in the ventral intraparietal area (VIP) (20), the dorsal medial superior temporal area (MSTd) (21), the lateral intraparietal area (LIP) (22, 23), and PMd (24, 25). Modeling work suggests that these complex coding schemes may help convert reference frames, optimally combine sensory information from different modalities, or perform nonlinear computations (15, 17, 26, 27). For example, MSTd cells nonlinearly combine signals encoding the head-centered position of the focus of visual expansion, eye position, and pursuit direction (28). Similarly, neurons in PMd, originally thought to use shoulder-centered coordinates (3), represent targets for arm movements in a variety of reference frames, including hand-centered, gaze-centered, and a frame related to eye, hand, and target positions, perhaps to flexibly compute optimal sensorimotor transformations for visually guided reaching (24, 25, 29).

In the present study, we revisited spatial coding in PRR during visually guided reaching. We found that, when eye and hand gain fields were explicitly differentiated from tuning shifts, PRR contained gaze-centered, hand-centered, and intermediate neurons. Thus, PRR neurons use idiosyncratic, nonsystematic reference frames, which are similar to those in PMd and other cortical areas. Yet, these same neurons also show a uniform and systematic gain field modulation. Eye and hand gain fields are systematically arranged within each individual neuron to form a compound gain field that encodes the distance between the point of the fixation and hand position (30). We suggest that nonsystematic and idiosyncratic organizational principles may increase computational flexibility, whereas systematic organizational principles increase computational efficiency. The brain simultaneously uses both principles within individual neurons of a single cortical area.

Results

We recorded from 259 isolated neurons in PRR (Fig. 1*D* and Fig. S1*A*) while monkeys planned and executed reaching movements. Our behavioral task and analyses were designed to identify the frames of reference used by cells in PRR and to distinguish shifts in tuning from gain field effects (30–32). Making this distinction requires that full tuning functions be obtained (Fig. 1*A*) (32). To accomplish this efficiently, we aligned a wide target array with each cell's preferred direction to capture the peak and both sides of the tuning function. Reaches were performed from different starting eye and hand positions to dissociate target position relative to fixation (gaze) from target position relative to the hand (Fig. 1*B*).

Author contributions: S.W.C.C. and L.H.S. designed research; S.W.C.C. performed research; S.W.C.C. analyzed data; and S.W.C.C. wrote the paper.

The authors declare no conflict of interest.

This article is a PNAS Direct Submission.

[1]To whom correspondence should be addressed. E-mail: steve.chang@duke.edu.

[2]Present address: Center for Cognitive Neuroscience, Duke Institute for Brain Sciences, Department of Neurobiology, Duke University School of Medicine, Durham, NC 27701.

This article contains supporting information online at www.pnas.org/cgi/content/full/0913209107/DCSupplemental.

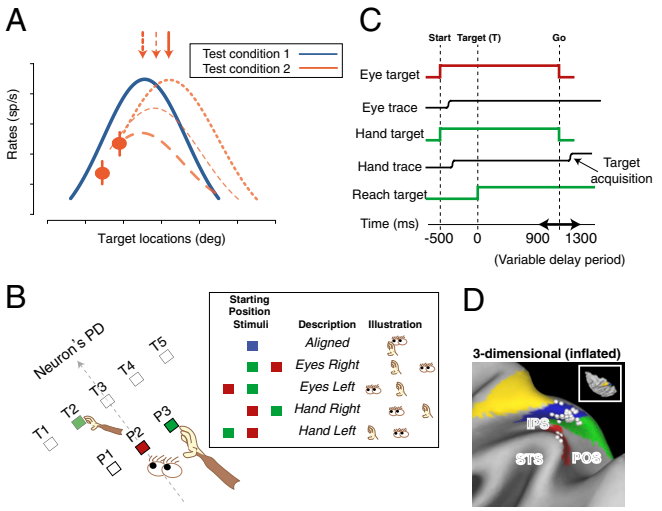

Fig. 1. Task design. (*A*) The importance of complete tuning curves when characterizing reference frames. Imagine that a complete curve is obtained in one condition (blue line), but only two data points are obtained in a second condition (orange points). The data could reflect a shift in reference frame (top dotted curve), a gain modulation (bottom dashed), or a combination of the two (middle dashed). The ambiguity would be resolved by collecting complete tuning curves or at least, the peak responses (arrows). (*B*) Behavioral task. Animals reached to one of eight target locations from one of five configurations of initial eye and hand positions (box). [Only five targets (*T1–T5*) near the neuron's preferred direction (PD) are shown]. *P1–P3* show potential starting eye and hand positions. All conditions and targets were fully interleaved. (*C*) The temporal sequence of the task, aligned on reach target onset (time 0). Start, onset of initial eye and hand targets; target (*T*), reach target onset; Go, go signal. (*D*) Recording sites from animal G shown on a map of inflated cortex (http://brainmap.wustl.edu/caret). Cortical areas are color coded according to Lewis and Van Essen (45). *Inset* shows the dorsal view. Green, PO/V6A (46); blue, MIP; yellow, dorsal area 5 (5D); red, lateral occipitoparietal area (LOP). Fig. S1*A* shows animal S.

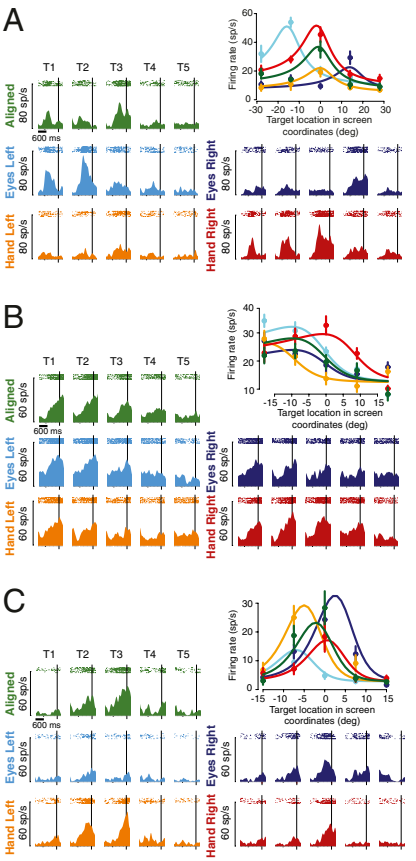

Fig. 2. Single cells. (*A*) Example PRR neuron with a gaze-centered frame of reference. Peri-stimulus time histograms and rasters are color coded for five test conditions and five target locations (box in Fig. 1*B*). Delay activity is shown with data aligned to the time of go cue (vertical line). (*Upper Right*) Color-coded mean firing rates (circles), SEM (bars), and fitted tuning curves are shown versus target locations in screen-centered coordinates. (*B*) An example neuron that encodes targets relative to the hand (hand-centered). (*C*) An example neuron using an intermediate representation (neither gaze- nor hand-centered). Fig. S2 shows target-aligned data.

We fitted cell activity to a nonlinear model with separate terms for linear eye and hand gain fields and a Gaussian tuning function for target position that could be gaze-centered, hand-centered, or intermediate (Eq. **1**). Animals successfully completed 89% and 96% of initiated trials (monkeys G and S, respectively), with median reach-response latencies of 238 ± 76 ms and 246 ± 55 ms (± SD). Table S1 summarizes median gaze and hand distance from the initial gaze targets, initial hand targets, and final reach targets.

Multiple Frames of Reference. Some neurons encoded target location relative to eye position (gaze-centered), others relative to initial hand position (hand-centered), and still others relative to a point lying along a line connecting the eye and hand positions (intermediate).

Consistent with previous reports (7, 24, 33), many PRR cells coded reach targets using a gaze-centered frame of reference (Fig. 2*A*). When the eyes and hand were aligned at the central position (*Aligned*), the delay period activity for the example neuron was strongest for the center target [*T3*; peak delay activity = 35.0 ± 5.8 sp/s (spikes/sec, mean ± SEM)]. When the starting eye position was displaced to the left (*Eyes Left*) or right (*Eyes Right*), peak delay activity was evoked by a target on the left (*T2*) or right (*T4*), respectively (53.9 ± 3.3 sp/s and 29.3 ± 4.4 sp/s). In contrast, when the starting hand position was displaced left or right, the peak remained at the center [*Hand Left* and *Hand Right* (19.1 ± 3.0 and 45.4 ± 5.2 sp/s, respectively)]. Tuning that shifts with eye position but not hand position is consistent with a gaze-centered representation (7, 24, 33).

We fitted the data to a nonlinear model that distinguishes gain fields from shifting reference frames (Eq. **1** and Fig. 2*A Upper Right*). A weight parameter identifies the location of the origin of each cell's frame of reference. A weight of 1 corresponds to an origin at fixation and therefore, describes a gaze-centered cell. A weight of 0 corresponds to an origin at the starting hand position and therefore describes a hand-centered cell. Finally, fractional weights correspond to origins lying along a line connecting the point of fixation with the starting hand position (a line intersecting *P1* and *P3* in Fig. 1*B*). For example, a weight of 0.5 corresponds to an origin midway between the eye and hand.

The weight parameter for the cell in Fig. 2*A* was 1.06 (not significantly different from 1; bootstrap test; $P < 0.05$). A stepwise regression analysis revealed that a purely gaze-centered model (retaining both eye and hand gain fields) (Eq. **2**) fit the data just as well as the full model (Eq. **1**) (F test; $P = 0.51$). The fit to the gaze-centered model included a 0.98 sp/s increase in firing for each degree of leftward eye position displacement (an eye position gain field) and a 1.01 sp/s per degree decrease for leftward hand displacement (a hand position gain field). The gaze-centered modulation had an amplitude of 34.7 sp/s. This reduced model accounts for 93.1% of the variance in firing (r^2). Multiplying the gaze-centered modulation by variance explained yields a "spike-variance explained" of 32.3 sp/s (*Methods*) (30). In comparison, the full model accounted for essentially the same amount of variance (93.3%), whereas a purely hand-centered

model (retaining both eye and hand gain fields) (Eq. **3**) accounted for only 70.4%.

If PRR neurons are involved in transforming gaze-centered into hand-centered representations, we might expect to find an explicit encoding of the latter in PRR. Consistent with this notion, although contrary to several previous reports (7, 24, 33) (but see ref. 34 and figure 4e in ref. 33), we found hand-centered representations in some cells (Fig. 2*B*). For the example cell, peak delay activity occurred for targets T1 and T2 for *Aligned*, *Eyes Left*, and *Eyes Right* conditions. In contrast, the tuning functions for *Hand Left* and *Hand Right* were shifted left and right, respectively. Tuning that shifts with hand but not eye position is consistent with a hand-centered representation of target position.

The weight parameter for this cell was 0.03 (not significantly different from 0; bootstrap test; $P < 0.05$). A stepwise regression analysis revealed that a purely hand-centered model (with eye and hand gain fields, Eq. **3**) fit the data just as well as the full model (F test; $P = 0.89$). There was a 0.45 sp/s per degree eye position gain field to the left and a 0.16 sp/s per degree hand position gain field to the right. The hand-centered modulation (15.7 sp/s) plus the eye and hand gain fields explain 82.2% of the variance or 12.9 sp/s of the spike-variance. In comparison, the full model accounted for essentially the same amount of variance (82.3%), whereas a purely gaze-centered model (with gain fields) (Eq. **2**) accounted for only 65.3%.

We also encountered cells that represented target locations in neither gaze- nor hand-centered coordinates (Fig. 2*C*). For the example cell, peak delay activities on both *Eyes Left* (9.5 ± 2.7) and *Hand Left* (25.0 ± 4.1) conditions were shifted slightly to the left compared with the *Aligned* condition, and peak activities on both *Eyes Right* and *Hand Right* conditions were shifted slightly to the right. The weight parameter for this cell was 0.63, corresponding to an intermediate representation (significantly different from both 0 and 1; bootstrap test; $P < 0.05$). A stepwise regression revealed that the full model (Eq. **1**) fit the data significantly better than either gaze- (Eq. **2**) or hand-centered (Eq. **3**) models ($P < 0.001$ for each F test). The full model revealed a 20.4 sp/s Gaussian modulation based on target position that was modulated by a 1.26 sp/s per degree rightward eye position gain field and a 0.81 sp/s per degree leftward hand position gain field. The mixed eye- and hand-centered modulation (20.4 sp/s) plus the eye and hand gain fields accounted for 85.3% of the total variance or 17.4 sp/s of the spike-variance. The gaze- and hand-centered models accounted for only 70.9% and 62.9%.

Population Analysis of Reference Frames. Fig. 3*A* shows the population distribution of the fitted reference frame (weight) parameter from all cells with at least 5 sp/s of spike-variance explained (103 of 259 cells). The modal value is just under 1 with a skew to the left and a median value of 0.72. The distribution of the fitted weights for all 255 cells for which the model converged looks similar to Fig. 3*A* and yields a similar median of 0.68 (Fig. S5). We classified cells by comparing fits to the full model (Eq. **1**) versus a gaze-centered (Eq. **2**) or hand-centered (Eq. **3**) model (stepwise regression). We found that 41% of 103 cells were gaze-centered (gaze model fit significantly better than the full model; F test; $P < 0.05$), 18% were hand-centered (hand model fit significantly better than the full model), and 21% were intermediate (neither reduced model fit significantly better than the full model). The remaining 20% of cells fit both reduced models better than the full model and therefore could not be classified (indeterminate).

Previous studies have reported different results at the population level (7, 24, 33). We, therefore, applied several alternative analyses to check our results. A Bayesian Information Criterion (BIC) analysis yielded similar results as the stepwise regression (42% gaze-centered, 21% hand-centered, and 37% intermediate

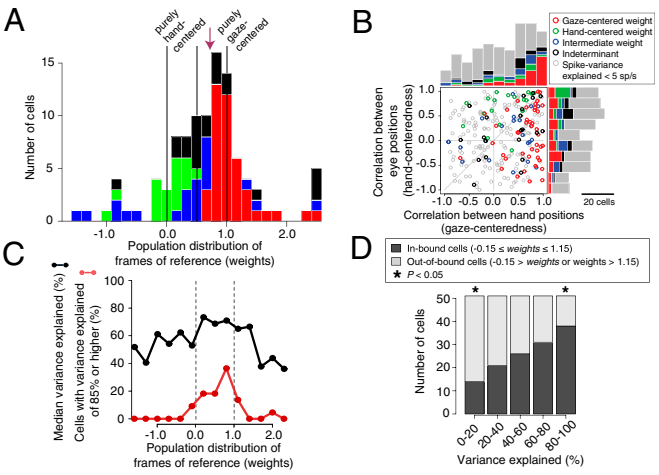

Fig. 3. Population. (*A*) The distribution of weights from the delay period (Eq. **1**). Cells with at least 5 sp/s of spike-variance explained are shown ($n = 103$; *Methods*). Bars are color coded based on a stepwise regression (see texts): red, gaze-centered; green, hand-centered; blue, intermediate; black, indeterminate. Vertical lines represent values corresponding to pure hand-centered (weight = 0), pure gaze-centered (1), and exactly halfway in between the two (0.5). Arrow, median. (*B*) Tuning shift analysis based on the cross-correlation method ($n = 259$). Correlation coefficients between two different hand positions (gaze-centeredness) and two different eye positions (hand-centeredness) are plotted. Cells with a spike-variance explained of at least 5 sp/s are color coded as in *A*. Cells with spike-variance explained of less than 5 sp/s are gray. (*C*) The variance explained (r^2; percent) by the full model (Eq. **1**) as a function of reference frame for all 255 fitted cells (black curve). Each data point represents the median variance explained for cells in a bin centered on the abscissa value of the point. The red curve shows the distribution of cells with an r^2 of 85% or higher; the area under the red curve sums to 100%. (*D*) Out-of-bound cells (weights <−0.15 or >1.15) are noisier than in-bound cells. All fitted cells were split into quintiles based on increasing variance explained. The plot shows the percentages of in-bound (dark bars) and out-of-bound (light bars) cells in each quintile. In-bound cells are overrepresented in the upper quintiles (high variance explained and therefore, less noisy), whereas out-of-bound cells are overrepresented in the lower quintiles. *$P <$ 0.05 by proportion test (Fig. S3 and S4).

cells) as did nonparametric permutation tests on the weight parameter (38% gaze, 12% hand, 24% intermediate, and 26% not classifiable). Similar results were obtained when the data from each animal were analyzed separately. Monkey G, with a right hemisphere chamber, showed a median weight of 0.70 with 39% gaze-centered, 18% hand-centered, and 20% intermediate cells (stepwise regression). Monkey S had a left hemisphere chamber and showed a median weight of 0.80 with 43% gaze-centered, 17% hand-centered, and 24% intermediate cells. Finally, we applied three previously published classification schemes (7, 23–25) for distinguishing gaze- and hand-centered frames of reference, and these confirmed our conclusion that PRR shows a broad range of representations, from gaze-centered to hand-centered, with a bias for gaze-centered cells (Fig. 3*B*, Fig. S6, and *SI Results*). We did not detect any anatomical segregation of cells as a function of their reference, or any clear evidence of temporal evolution of coding schemes (Fig. S9, *SI Text*).

Intermediate Representations. Gaze- and hand-centered representations have clear correlates in the physical world. The early visual system is gaze-centered by construction, and a high-level motor representation for reaching might reasonably be expected to be hand-centered. In contrast, the existence of intermediate representations is nonintuitive. Despite their name, it is not at all obvious that intermediate reference frames constitute computational intermediaries in the conversion from one frame of reference to another. In two dimensions, the transformation between

gaze- and hand-centered frames requires only the subtraction of two vectors, a simple linear operation (35). A feed-forward three-layer neural network trained using back-propogation accomplishes this using gaze-centered, gain-modulated nodes, not intermediate coding (11, 12, 14, 16, 17, 30, 36, 37). Although it is true that neural networks can be designed to produce intermediate representations (15, 17, 26), it nonetheless behooves us to ask if intermediate representations might be artifactual.

Might recording spikes from two incompletely isolated neurons, one with gaze-centered encoding and one with hand-centered encoding, produce an intermediate representation? Mathematically, a weighted sum of gaze- and hand-centered representations is quite different from an intermediate representation. However, it is not clear how our classification schemes would respond to a weighted sum. We tested if neurons that were classified as intermediate by the stepwise regression test would be better fit by a weighted sum of a gaze-centered and a hand-centered representation. We found that this was not the case. Of 22 intermediate cells that met the 5 sp/s spike-variance explained criterion, all but two cells (91%) were better fit by the intermediate model compared with a weighted sum model (BIC). Of all intermediate cells ($n = 44$), only 5% were better fit by the weighted sum. This effectively rules out poor isolation as an explanation for intermediate cells.

A second way that an artifactual intermediate representation might occur is by adding noise to a gaze- or hand-centered neuron. If intermediate neurons were merely noisy (hence, misclassified) gaze- or hand-centered cells, then we would expect that our model would explain less variance in intermediate cells compared with gaze- and hand-centered cells. This was not the case. The black line in Fig. 3*C* shows the median percentage of variance explained for all cells as a function of their frame of reference. The line is approximately flat between 0 and 1, not U-shaped. In particular, cells in the bin centered on $x = 0.5$ (weights from 0.35 to 0.65) have a median variance explained similar to that of cells with weights close to 0 or 1. This strongly suggests that intermediate cells do not, in general, result from noisy observations of gaze- or hand-centered cells.

Although the majority of cells have weights close to or between 0 and 1, many weights fall well outside these boundaries. Such cells have also been reported in previous studies (17, 20, 21). There is no a priori reason to believe that out-of-bound representations (weights substantially less than 0 or substantially greater than 1) should differ from in-bound representations (weights within or near the interval from 0 to 1). In fact, an independent simulation study was able to produce both in-bound and out-of-bound representations (17). Interestingly, Fig. 3*C* shows that our model explains more variance for in-bound cells compared with out-of-bound cells. The three highest values of median variance explained occur for cells with weights between 0.05 and 0.95. This pattern is even clearer in the distribution of cells with high variance explained: 95% of cells with a variance explained of at least 85% have weights between −0.15 and 1.15 (red line in Fig. 3*C* and Fig. S7).

To compare the goodness of fit for in-bound and out-of-bound cells in detail, we divided all cells into five quintiles of variance explained and then determined the proportion of in-bound and out-of-bound cells in each quintile (Fig. 3*D*). If out-of-bound cells were no different from in-bound cells, we would expect equal representation in each. Instead, in-bound cells were overrepresented in the upper quintile(s), whereas out-of-bound cells were overrepresented in the lower quintile(s). We found a similar pattern in spike-variance explained (Fig. S3*A*). This suggests that out-of-bound intermediate cells are different from in-bound intermediate cells.

Might noise artifactually produce out-of-bound cells? We injected Gaussian noise (mean = 0 sp/s; SD = 5 sp/s) into all well-fit in-bound cells ($n = 130$) (Fig. S4*A*) to see if it might cause in-bound cells to be reclassified as out-of-bound cells. Surprisingly, 48 (37%) of the in-bound cells became out-of-bound when noise was added (Fig. S4*B*). With still more noise (SD = 15 sp/s), 76 (58%) of in-bound cells were reclassified as out-of-bound cells (Fig. S4*B*). The most parsimonious explanations of our data are, therefore, that the out-of-bound cells that we observe arise as an artifact from the corruption of in-bound cells (gaze-centered, hand-centered, and in-bound intermediate cells) by noise. However, we cannot eliminate the alternative possibility that the models that we have used (Eqs. **1–5**) are inappropriate for out-of-bound cells (i.e., out-of-bound cells encode spatial information in a fundamentally different way).

Reference Frames and Eye and Hand Gain Fields. A gain field occurs when tuned responses are scaled as a function of a postural variable (38, 39). Simulations show the potential utility of gain fields in a number of neural computations, including reference frame transformations (11, 12, 14, 16, 17, 36). Recently, we reported that PRR neurons are modulated by a compound gain field: eye and hand position gain fields with similar magnitudes but opposite signs (30). This compound gain field effectively modulates responses in proportion to the distance between the point of visual fixation and the hand (eye-hand distance) (Eq. **5**) (30). Across neurons with at least 5 sp/s of spike-variance explained, the median absolute eye gain field was 3.44% of peak activity per degree, and the median absolute hand gain field was 2.08% per degree. Within each cell, eye and hand gain fields were negatively correlated (Spearman's rank correlation; $r = -0.61$; $P < 0.00001$; type II regression slope = −0.74) (Fig. 4). Only 4 of 103 cells showed a significant difference (two-tailed t test; $P < 0.05$) between the fitted eye position gain field parameter and the negative of the fitted hand position gain field parameter.

We now report that there is no systematic relationship between gain fields and frames of reference in PRR. One could imagine that eye–hand distance gain fields might occur only in gaze-centered neurons and not in neurons in which the eye–hand distance has already been combined with visually derived target information to produce a hand-centered representation of the target. This was not the case. Hand-centered (weight close to 0), gaze-centered (weight close to 1), and in-bound intermediate neurons (intermediate weights that fall inside of 0 and 1) all showed similar gain fields (Fig. S8*A*). The match between eye and hand gain fields (i.e., offset from the negative unity line in Fig. 4) was consistent across all cell types with a median unsigned mismatch of 1.1% change in activity per degree for gaze-centered neurons, 1.2% per degree for hand-centered neurons, and 1.6 per degree for in-bound intermediate neurons ($P > 0.7$ for all comparisons; Wilcoxon rank sum test) (Fig. S8*B*). The gain field mismatch for out-of-bound neurons was 3.1 per degree (i.e., much larger than the mismatch for in-bound cells), which is consistent with the idea that out-of-bound cells represent either corrupted recordings of in-bound cells or a separate pop-

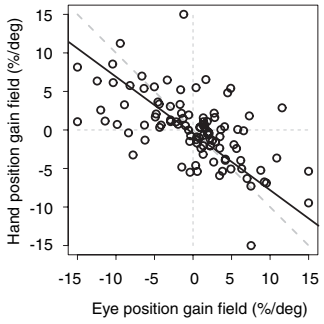

Fig. 4. The compound eye–hand distance gain field. Eye and hand position gain field amplitudes (percent per degree) tend to be similar in magnitude but opposite in sign for single neurons (30). Solid black line, type II regression; dashed diagonal line, negative unity line.

ulation with an encoding scheme not captured by our model (*SI Text* and Fig. S3*B*).

Discussion

PRR neurons have been implicated in transforming gaze-centered target locations into hand-centered locations (5, 31, 33, 40–42). Previous studies report a predominantly gaze-centered coding (7, 24, 33), although individual hand-centered cells have been observed (34) (figure 4*e* in ref. 33). We revisited this issue using a behavioral paradigm and analysis specifically designed to distinguish shifts in tuning from gain field modulations (30, 32). For each cell, we collected full tuning curves, and analyzed the data using a family of nonlinear models with explicit tuning and gain-field terms (Eqs. **1**–**5**). We found that reference frames in PRR are idiosyncratic to each neuron, ranging continuously from gaze-centered to hand-centered, and they include many cells with intermediate representations (Figs. 2*C* and 3*A* and Fig. S5). These intermediate representations are reminiscent of the mixed gaze- and head-centered reference frames found in other parts of the PPC (18–20, 23, 32).

A continuous distribution of reference frames has been reported in area PMd, an area to which PRR projects (8, 25, 43). In PRR the distribution is strongly biased to gaze-centered cells (Fig. 3*A*), whereas in PMd, the distribution is biased to hand-centered cells (25). This difference may reflect a gradual transformation from an initial sensory (gaze-centered) frame in PRR to a more motor frame in PMd. Such a bias is consistent with the notion that visuomotor neurons represent information in multiple, differentially weighted frames of reference (29). Although their function remains unclear, intermediate representations are thought to play a critical role, perhaps mediating nonlinear computations required for 3D coordinate frame transformations or assisting in optimal cue combination (13, 15, 17, 26, 27).

We distinguish in-bound cells, where a change in eye or hand position produces a comparable or smaller shift in tuning, from out-of-bound cells, whose tuning shifts by an amount greater than the change in eye or hand position (rogue cells) (44). Out-of-bound cells have been found in reference frame studies in VIP and in simulation studies (17, 20, 21). In PRR, we find that the goodness of fit for in-bound intermediate cells is comparable with that of pure gaze- and hand-centered cells. In contrast, out-of-bound intermediate neurons are less well fit by our model and either arise artifactually from noisy recordings of in-bound neurons or encode spatial information in an entirely different manner from in-bound neurons.

Our approach is ideal for cells whose responses are peaked in space. For cells that are monotonically tuned or cells for which we sampled only a monotonic portion of the response field because of poor positioning of the target array, our model cannot accurately distinguish gain modulations from tuning shifts. This was only a minor issue for us, because 91% of our cells showed a clear peak. A second caveat is that we assume that gain fields are linear, yet cannot distinguish linear from nonlinear gain fields using our data. Except in extreme cases (e.g., U-shaped gain fields), the linear assumption is a good first approximation (38, 39). A final caveat is that our task was designed to test only gaze- and hand-centered frames of reference. Although we found little evidence for head-, body-, or world-centered frames, still other frames are possible.

The continuous distribution of idiosyncratic reference frames for target position stands in contrast to the systematic and uniform organization of eye and hand gain fields in PRR. Eye and hand gain fields are systematically coupled to one another such that every cell is modulated by eye–hand distance (30). Gain fields are not identical across cells. There is a small and idiosyncratic mismatch of eye and hand gain fields within each cell, and the magnitude and even the sign of the compound gain field varies from cell to cell (e.g., some cells are more active when the hand is to the right of fixation and less active when the hand is to the left of fixation, and vice versa). Despite this variability, however, there is a clear underlying organization; there are very few cells in which eye and hand gain fields either both increase or both decrease for rightward movements, for example. This systematic organization is strong evidence that gain fields are purposeful computational elements and not accidental or incidental modulations (17).

Thus, one dimension of coding in PRR (reference frame) is continuous and idiosyncratic within each cell, whereas another dimension (the compound eye and hand gain field) is organized systematically. We suggest that an apparently haphazard organization, such as is seen with frames of reference in many brain areas, occurs when encoding signals that will be used for multiple different and perhaps nonlinear computations. In contrast, a systematic organization, such as is seen with eye and hand gain fields, occurs when encoding signals that will be used for a small number of fairly linear computations.

Methods

Data Analysis. The mean spike rate was computed in a 700-ms delay period (850 ms before the time of the go signal to 150 ms before the time of the go signal). Similar results were obtained using slightly different time intervals and alignment points (e.g., from 150 ms to 850 ms after target onset). We fitted mean spike rates in 25 different conditions (5 initial conditions × 5 targets) to a nonlinear seven-parameter Gaussian model:

$$Firing\ rate = pa \times exp^{\frac{-(\theta - mid)^2}{2 \times sd^2}} \times \left(1 + E \times g_{Eye} + H \times g_{Hand}\right) + k, \quad [1]$$

$$where\ \theta = tan^{-1}\left(\frac{T - (weight \times E + (1 - weight) \times H)}{ecc}\right)$$

We refer to Eq. **1** as the full model. The fit was performed using the nls function in the R statistics package (www.R-project.org). The model inputs were firing rates, target eccentricity (ecc), target displacement (T), and the displacement of eye (E) and hand target (H). The output parameters were baseline (k), peak amplitude modulation (pa), offset of the center of the tuning curve from the central target (T3; mid), standard deviation (sd) of the Gaussian curve in degrees of visual angle, the amplitudes of the eye position gain field (gEye) and the hand position gain field (gHand; both in fractional modulation per degree), and a unitless weight parameter (weight), which described the frame of reference for each cell, with weights of 1 and 0 corresponding to pure gaze- and hand-centered cells, respectively. See *SI Text* for details on model parameters.

The gaze-, hand-, and head/body/world-centered models are each identical to the full model except for their respective θ terms:

$$\theta = tan^{-1}\left(\frac{T - E}{ecc}\right); \quad \theta = tan^{-1}\left(\frac{T - H}{ecc}\right), \quad [2\text{–}3]$$

$$\theta = tan^{-1}\left(\frac{T}{ecc}\right). \quad [4]$$

The following equation replaces the two separate eye and hand gain field terms with a single distance gain field term, reducing the number of parameters to six (30):

$$Firing\ rate = pa \times exp^{\frac{-(\theta - mid)^2}{2 \times sd^2}} \times \left(1 + (E - H) \times g_{Diff}\right) + k \quad [5]$$

Selection Criteria. A total of 259 neurons were recorded from PRR in two monkeys. For each signal that we encountered, we used the mapping task to ascertain isolation, stability, and approximate preferred direction of that cell. For each stable, well-isolated single neuron that showed clear spatial tuning in the mapping task (n = 259), we ascertained the preferred direction from the mapping task and then, ran the main task. These 259 cells reported here represent about 60% of the ~450 signals that we encountered. About 30% of signals were rejected because of poor iso-

lation or stability, and the remaining 10% were rejected because of absent or unclear spatial tuning. In this report, we analyze the data of every one of the 259 cells in which we decided to run the main task. Because the decision to run or not run this task in a given cell was based solely on the results of the mapping task, the only bias in cell selection was in favor of cells with spatial tuning.

Model fits were judged based on how well the model accounted for firing rate. We took both the strength of the Gaussian tuning and the overall variance explained by the model into account. We combined these two factors into a single measure by multiplying variance explained (r^2) by the peak modulation of the Gaussian fit (sp/s) to obtain spike-variance explained (sp/s) (30). We accepted neurons with a criterion value of 5 sp/s of spike-variance explained (n = 103). Acceptance based on different criterion values of spike variance explained, variance explained alone, or χ^2 tests of the goodness of fit all resulted in similar conclusions. *SI Text* contains more detailed methods.

ACKNOWLEDGMENTS. We thank D. Angelaki, S. Wise, A. Batista, and V. Rao for helpful discussions, G. DeAngelis for help with designing the experiment, T. Malone, J. Vytlacil, and J. Baker for magnetic resonance imaging and localization, and E. Proctor and T. Shew for technical assistance. This work was supported by National Eye Institute Grant R01 EY012135.

1. Robinson DA (1981) The use of control systems analysis in the neurophysiology of eye movements. *Annu Rev Neurosci* 4:463–503.
2. Kalaska JF, Scott SH, Cisek P, Sergio LE (1997) Cortical control of reaching movements. *Curr Opin Neurobiol* 7:849–859.
3. Caminiti R, Johnson PB, Galli C, Ferraina S, Burnod Y (1991) Making arm movements within different parts of space: The premotor and motor cortical representation of a coordinate system for reaching to visual targets. *J Neurosci* 11:1182–1197.
4. Flanders M, Helms T, Stephen I, Soechting, JF (1992) Early stages in a sensorimotor transformation. *Behav Brain Sci* 15:309–320.
5. Snyder LH (2000) Coordinate transformations for eye and arm movements in the brain. *Curr Opin Neurobiol* 10:747–754.
6. Crawford JD, Medendorp WP, Marotta JJ (2004) Spatial transformations for eye-hand coordination. *J Neurophysiol* 92:10–19.
7. Batista AP, Buneo CA, Snyder LH, Andersen RA (1999) Reach plans in eye-centered coordinates. *Science* 285:257–260.
8. Johnson PB, Ferraina S, Bianchi L, Caminiti R (1996) Cortical networks for visual reaching: Physiological and anatomical organization of frontal and parietal lobe arm regions. *Cereb Cortex* 6:102–119.
9. Poggio T, Edelman S (1990) A network that learns to recognize three-dimensional objects. *Nature* 343:263–266.
10. Poggio T (1990) A theory of how the brain might work. *Cold Spring Harb Symp Quant Biol* 55:899–910.
11. Zipser D, Andersen RA (1988) A back-propagation programmed network that simulates response properties of a subset of posterior parietal neurons. *Nature* 331: 679–684.
12. Burnod Y, et al. (1992) Visuomotor transformations underlying arm movements toward visual targets: A neural network model of cerebral cortical operations. *J Neurosci* 12:1435–1453.
13. Carrozzo M, Lacquaniti F (1994) A hybrid frame of reference for visuo-manual coordination. *Neuroreport* 5:453–456.
14. Salinas E, Abbott LF (1995) Transfer of coded information from sensory to motor networks. *J Neurosci* 15:6461–6474.
15. Pouget A, Snyder LH (2000) Computational approaches to sensorimotor transformations. *Nat Neurosci* 3 (Suppl):1192–1198.
16. Smith MA, Crawford JD (2005) Distributed population mechanism for the 3-D oculomotor reference frame transformation. *J Neurophysiol* 93:1742–1761.
17. Blohm G, Keith GP, Crawford JD (2009) Decoding the cortical transformations for visually guided reaching in 3D space. *Cereb Cortex* 19:1372–1393.
18. Jay MF, Sparks DL (1987) Sensorimotor integration in the primate superior colliculus. II. Coordinates of auditory signals. *J Neurophysiol* 57:35–55.
19. Metzger RR, Mullette-Gillman OA, Underhill AM, Cohen YE, Groh JM (2004) Auditory saccades from different eye positions in the monkey: Implications for coordinate transformations. *J Neurophysiol* 92:2622–2627.
20. Avillac M, Denève S, Olivier E, Pouget A, Duhamel JR (2005) Reference frames for representing visual and tactile locations in parietal cortex. *Nat Neurosci* 8:941–949.
21. Fetsch CR, Wang S, Gu Y, Deangelis GC, Angelaki DE (2007) Spatial reference frames of visual, vestibular, and multimodal heading signals in the dorsal subdivision of the medial superior temporal area. *J Neurosci* 27:700–712.
22. Stricanne B, Andersen RA, Mazzoni P (1996) Eye-centered, head-centered, and intermediate coding of remembered sound locations in area LIP. *J Neurophysiol* 76: 2071–2076.
23. Mullette-Gillman OA, Cohen YE, Groh JM (2005) Eye-centered, head-centered, and complex coding of visual and auditory targets in the intraparietal sulcus. *J Neurophysiol* 94:2331–2352.
24. Pesaran B, Nelson MJ, Andersen RA (2006) Dorsal premotor neurons encode the relative position of the hand, eye, and goal during reach planning. *Neuron* 51: 125–134.
25. Batista AP, et al. (2007) Reference frames for reach planning in macaque dorsal premotor cortex. *J Neurophysiol* 98:966–983.
26. Pouget A, Deneve S, Duhamel JR (2002) A computational perspective on the neural basis of multisensory spatial representations. *Nat Rev Neurosci* 3:741–747.
27. Xing J, Andersen RA (2000) Models of the posterior parietal cortex which perform multimodal integration and represent space in several coordinate frames. *J Cogn Neurosci* 12:601–614.
28. Ben Hamed S, Page W, Duffy C, Pouget A (2003) MSTd neuronal basis functions for the population encoding of heading direction. *J Neurophysiol* 90:549–558.
29. McGuire LM, Sabes PN (2009) Sensory transformations and the use of multiple reference frames for reach planning. *Nat Neurosci* 12:1056–1061.
30. Chang SW, Papadimitriou C, Snyder LH (2009) Using a compound gain field to compute a reach plan. *Neuron* 64:744–755.
31. Marzocchi N, Breveglieri R, Galletti C, Fattori P (2008) Reaching activity in parietal area V6A of macaque: Eye influence on arm activity or retinocentric coding of reaching movements? *Eur J Neurosci* 27:775–789.
32. Mullette-Gillman OA, Cohen YE, Groh JM (2009) Motor-related signals in the intraparietal cortex encode locations in a hybrid, rather than eye-centered reference frame. *Cereb Cortex* 19:1761–1775.
33. Buneo CA, Jarvis MR, Batista AP, Andersen RA (2002) Direct visuomotor transformations for reaching. *Nature* 416:632–636.
34. Batista AP (1999) Contributions of parietal cortex to reach planning. PhD dissertation (California Institute of Technology, Pasadena, CA).
35. Bullock D, Grossberg S (1988) Neural dynamics of planned arm movements: Emergent invariants and speed-accuracy properties during trajectory formation. *Psychol Rev* 95: 49–90.
36. Salinas E, Abbott LF (1996) A model of multiplicative neural responses in parietal cortex. *Proc Natl Acad Sci USA* 93:11956–11961.
37. Blohm G, Crawford JD (2007) Computations for geometrically accurate visually guided reaching in 3-D space. *J Vis* 7:1–22.
38. Salinas E, Thier P (2000) Gain modulation: A major computational principle of the central nervous system. *Neuron* 27:15–21.
39. Andersen RA, Mountcastle VB (1983) The influence of the angle of gaze upon the excitability of the light-sensitive neurons of the posterior parietal cortex. *J Neurosci* 3: 532–548.
40. Galletti C, Fattori P, Kutz DF, Battaglini PP (1997) Arm movement-related neurons in the visual area V6A of the macaque superior parietal lobule. *Eur J Neurosci* 9:410–413.
41. Shadmehr R, Wise SP (2005) *The Computational Neurobiology of Reaching and Pointing: A Foundation for Motor Learning* (MIT Press, Cambridge, MA), pp xvii–575.
42. Chang SW, Dickinson AR, Snyder LH (2008) Limb-specific representation for reaching in the posterior parietal cortex. *J Neurosci* 28:6128–6140.
43. Tanné J, Boussaoud D, Boyer-Zeller N, Rouiller EM (1995) Direct visual pathways for reaching movements in the macaque monkey. *Neuroreport* 7:267–272.
44. Arnold DB, Robinson DA (1991) A learning network model of the neural integrator of the oculomotor system. *Biol Cybern* 64:447–454.
45. Lewis JW, Van Essen DC (2000) Mapping of architectonic subdivisions in the macaque monkey, with emphasis on parieto-occipital cortex. *J Comp Neurol* 428:79–111.
46. Galletti C, Fattori P, Kutz DF, Gamberini M (1999) Brain location and visual topography of cortical area V6A in the macaque monkey. *Eur J Neurosci* 11:575–582.

Supporting Information

Chang and Snyder 10.1073/pnas.0913209107

SI Results

Population Analyses Using Alternative Metrics. We feel strongly that fitting data to an explicit and flexible model is a powerful way to characterize cells and determine their frame of reference (Fig. 3*A* and Fig. S5). However, because our findings of hand-centered and intermediate neurons conflict with previous conclusions drawn from parietal reach region (PRR), we performed three additional analyses, taken from the previously published studies of reference frames for reaching, that were not based on models (1–4).

First, we correlated activity between a pair of conditions with different starting eye positions (*Eyes Left* and *Eyes Right*) and between a pair of conditions with different starting hand positions (*Hand Left* and *Hand Right*) (2, 3). The pattern of activity of gaze-centered cells would be relatively unaffected by change in hand position and therefore would show high correlation coefficients (little change) between *Hand Left* and *Hand Right* conditions (abscissa of Fig. 3*B*; a measure of gaze-centeredness). In contrast, gaze-centered cells would be substantially affected by a change in eye position and therefore would show low correlation coefficients between *Eyes Left* and *Eyes Right* conditions (ordinate is a measure of hand-centeredness). Hand-centered cells would show the opposite pattern—low correlations between *Hand Left* and *Hand Right* responses and high correlations between *Eyes Left* and *Eyes Right* responses. Because correlations are scale-invariant, gain field modulation should have minimal effect on these patterns.

Of all 259 cells, 52% showed more positive correlations for gaze-centeredness than hand-centeredness (points below the diagonal in Fig. 3*B*). The results of this analysis roughly matched our classification results using an explicit model: cells with weights close to 1 (red) tend to have high gaze-centeredness, and cells with weights close to 0 (green) tend to have high hand-centeredness. In particular, 81% of the cells that we classified as gaze centered (Fig. 3*A*) fell below the diagonal line in Fig. 3*B*, and 94% of hand-centered cells fell above the diagonal line. However, the cells that we classified as intermediate (blue) or indeterminate (black) were evenly distributed across the plot; they did not lie close to the diagonal line as one might expect. Thus, the correlation metric agrees with the explicit model in identifying the presence of both gaze- and hand-centered neurons in PRR. However, the correlation metric does not clearly identify intermediate or unclassifiable cells. Furthermore, although the metric may be robust to the presence of gain fields, it provides no information about them (in contrast to fitting the data to an explicit model that includes gain-field terms).

Second, we calculated a Euclidean distance metric to quantify the sensitivity of neuronal responses to different target locations with changing eye or hand positions (Eq. **S1**) (4). This method is conceptually similar to the correlation method, but it uses a simpler metric for comparing responses with a set of targets across two conditions (e.g., *Eyes Left* and *Eyes Right*). Briefly, the Euclidean distance for individual cells was computed using

$$\textit{Euclidean distance} = \frac{\sqrt{\sum_{i=1}^{T}(n-m)^2}}{\sqrt{T}}, \qquad \textbf{[S1]}$$

where T represents the number of target locations, n and m represent neuronal responses for different starting eye positions (in case of computing Euclidean distance for different eye positions) or different starting hand positions (in case of computing the distance for different hand positions). The responses n and m are normalized to a scale of 0–1 by subtracting the minimum response and then, dividing by the maximum response, resulting in a metric that is 0 if the responses are identical and 1 if they are maximally different (ref. 4 has further details).

Like the correlation analysis, this analysis showed a distribution of eye and hand sensitivity with more sensitivity to changes in eye position than hand position (mean difference of 0.04 on a scale of 0–1; $P < 0.005$; two-tailed t test). Just over one-half of the 259 cells (56%) were more sensitive to changes in eye position (Fig. S6*A*, points below the diagonal), whereas 44% were more sensitive to changes in hand position (points above the diagonal). This was the reverse of the pattern seen in dorsal premotor cortex (PMd), where 42% and 58% of cells were more sensitive to eye and hand positions, respectively (4). Of the well-fit cells, 65% were more sensitive to changes in eye position, and 35% were more sensitive to changes in hand position, again showing a gaze-centered bias (difference of 0.07; $P < 0.0005$). The results closely matched those of the explicit model with 90% of cells modeled as gaze-centered (red) falling below the diagonal and 94% of the cells modeled as hand-centered (green) falling above the diagonal (Fig. S6*A*). Intermediate and indeterminate cells tended to fall near the diagonal. Thus, the Euclidean distance method compares well with the explicit model.

Third, we subjected our data to a singular value decomposition (1). We constructed two matrices for each cell: one response matrix based on different target locations for different starting eye positions and the other based on different target locations for different starting hand positions. We then obtained sets of three ordered singular values (σ_i) for unique eye and hand positions. Using the three singular values, we computed a separability index (α) for eye and hand (Eq. **S2**):

$$\alpha = \frac{\sigma_1^2}{\sum_i^3 \sigma_i^2}. \qquad \textbf{[S2]}$$

To determine whether target and eye position or target and hand position are significantly separable, we performed a permutation test ($P < 0.05$) to obtain 95% confidence intervals for each pair for each cell. A gaze-centered cell would show a higher separability index for target and hand positions than for eye and target positions, and a hand-centered cell would show the opposite. In the population ($n = 259$), 65% of cells showed higher indices for target and hand positions than for target and eye positions (i.e., more gaze-centered than hand-centered), and this bias was itself significant ($P < 0.01$; two-tailed t test) (Fig. S6*B*). Target and eye positions were inseparable for 42% of cells (259 cells total; analogous to gaze-centered), whereas target and hand positions were inseparable for 18% of cells (analogous to hand-centered; permutation test; $P < 0.05$). Twenty percent of cells showed inseparability for target and eye as well as for target and hand positions (analogous to intermediate), and the remaining 20% of cells were separable for target and eye as well as for target and hand (indeterminate; permutation test). The results were similar to those from our explicit modeling (Fig. 3*A*): 88% of gaze-centered cells showed higher indices of target and hand position pairs, and 78% of hand-centered cells showed higher target and eye position pairs. Intermediate and indeterminate cells were often but not always close to the diagonal (Fig. S6*B*).

Overall, these additional metrics support our finding of both gaze- and hand-centered neurons in PRR with a bias to gaze-centered and continuous, rather than bimodal, distribution of properties, which is consistent with the existence of intermediate cells.

An ANOVA has also been used to identify the frame of reference used by particular cells. Briefly, the data are subjected to a two-way analysis with factors of gaze-centered target position, hand-centered target position, eye position, and hand position. We find that many cells show a significant effect by ANOVA but on inspection, show no coherent pattern of responses. In our hands, ANOVA provided inferior results, and we, therefore, did not consider it (see below).

Out-of-Bound Cells and Eye–Hand Distance Gain Field. In contrast to in-bound cells, out-of-bound neurons showed significantly greater mismatch between eye and hand gain fields compared with in-bound neurons (Fig. S3*B*). The median absolute mismatch for in-bound and out-of-bound cells was 1.2 and 3.1% per degree, respectively ($P < 0.005$; Wilcoxon rank sum test). Consistent with this, in-bound cells were overrepresented in the lower quintile(s) of mismatch, whereas out-of-bound cells were overrepresented in the upper quintile(s) of mismatch (Fig. S3*B*).

Temporal Stability of Reference Frame. If PRR transforms a target representation from one uniform frame of reference (e.g., gaze-centered) to another uniform frame of reference (e.g., hand-centered), it is reasonable to hypothesize that a reference frame used in an early portion of the delay period might be gaze-centered, whereas a reference frame used in a late portion of the delay period might be hand-centered. To address this, we examined the distribution of reference frames at sequential time intervals throughout the duration of the task (200 ms sliding window at a 50-ms step size). We included cells in this analysis as long as they showed at least 5 sp/s of spike-variance explained at any of the sampled 200-ms time windows. Population median weights across different time intervals remained stable throughout the task (Fig. S9). We also examined changes in the model-derived weight parameter relative to the median weight of our population, 0.72 (Fig. 3*A* and solid line in Fig. S9). Throughout different time epochs, reference frames did not change relative to the population's median weight (two-tailed t test; $P < 0.05$).

Even in the absence of the population-level temporal evolution, individual cells may still dynamically alter their reference frames over time in a more or less balanced way. To test this, we examined the proportion of cells with significant changes in the weight parameter of the general model (Eq. **1**) between a visual interval (from 50 to 250 ms relative to target onset) and premovement interval (last 200 ms before movement onset). We found that only 12% of those cells with at least 5 sp/s spike-variance explained in both task epochs (11/89 cells) showed a significant change in weight between the two intervals (bootstrap test; $P < 0.05$).

Therefore, consistent with the previous report by Buneo et al. (5), we did not observe clear evidence that the reference frames in PRR dynamically evolve over time. At best, we saw only small and nonsystematic fluctuations over the course of a trial (Fig. S9). This suggests that PRR neurons seem to use diverse, nonuniform reference frames throughout motor planning.

Additional Analysis. Cells with broad tuning may have a different relationship between reference frames and gain fields compared with more narrowly tuned cells. To examine this, we repeated our main analysis separately for cells with tuning widths either greater or less than 40°. The resulting distributions of weights were not significantly different from each other ($P = 0.31$; Wilcoxon signed rank), with median weights of 0.77 ± 0.12 for broadly tuned cells and 0.65 ± 0.09 for narrowly tuned cells. Similarly, the negative coupling of eye and hand gain fields was present in both populations: $r = -0.60$ and -0.59 for the broadly and narrowly tuned cells, respectively (Spearman's rank correlation).

Another method of selecting the cells to include is to show a significant effect in a multiway ANOVA with factors of target position relative to eye, target position relative to hand, eye position, and hand position. Fig. S7*A* shows variance explained (*Upper*) and spike-variance explained (*Lower*) as a function of the weight parameter of our model; color coding indicates cells that passed a 5 sp/s spike-variance explained criterion or an ANOVA criterion ($P < 0.001$). Fig. S7*B* shows similar data using a less strict significance criterion for the ANOVA ($P < 0.05$). These plots show that, even at the $P < 0.001$ level, the ANOVA test would include many cells with very low variance explained or low spike-variance explained. There are two possible interpretations of these results. The interpretation that we prefer is that ANOVA is overly sensitive to changes in firing. Because no systematic model is applied, even a nonsystematic deviation in firing in one or more of the test conditions will be taken as evidence for sensitivity to eye or hand position. Alternatively, one can argue that the positive ANOVA in the presence of low variance or spike-variance explained means that there is a source of variation in the data that our model does not capture. This is true almost by definition but does not address if the variation is systematic in relation to a variable of interest.

Finally, some cells might use a frame of reference that is insensitive to both eye and hand positions (e.g., a head-, body-, or world-centered frame). We tested this by comparing fits to the full model (**Eq. 1**) and a reduced model in which target angle was computed relative to the (fixed) head and body orientation (**Eq. 4**). Of cells that fit at least one model with at least 5 sp/s spike-variance explained ($n = 108$), the full model explained the data significantly better in 85% of cells (BIC). Therefore, a frame of reference that is insensitive to eye and hand position (e.g., a head-, body- or world-centered frame of reference) cannot account for the vast majority of cells in PRR.

SI Discussion

Accumulating evidence suggests that intermediate frames of reference are common in both sensory and motor regions of the brain. In the intraparietal sulcus (IPS), it has been suggested that posterior parietal neurons use reference frames that are intermediate between gaze- and head-centered for encoding locations for saccades to auditory or visual targets (3, 6, 7). In particular, Mullette-Gillman et al. (3, 7) recorded from the lateral intraparietal area (LIP) and the medial bank of the IPS located across from LIP, regions distinct from PRR, in an auditory and visual saccade task and found that these neurons use mixed frames of reference for encoding target locations (i.e., reference frames in these neurons ranged from gaze- to head-centered and often showed mixed coding schemes for encoding saccade target locations in space) (3, 7). Cells in the superior and inferior colliculus use neither a purely gaze- nor a purely head-centered frame of reference for encoding the location of auditory targets (8–10). The ventral intraparietal area (VIP) and the dorsal medial superior temporal area (MSTd) cells use reference frames that range from gaze- to head-centered for integrating visual and tactile information (11) and for integrating visual and vestibular information (12), respectively. Early studies in PMd reported the use of a uniform hand-centered frame of reference (13, 14). Two recent studies, however, refute this claim. One study reported complex, mixed reference frames in PMd, with some cells using a hand-centered frame of reference and others using a gaze-centered frame; many (52%) used neither a hand- nor a gaze-centered frame (4). Another study reported that PMd neurons encode relative spatial relationships among eye, hand, and target positions in 1D or 2D (1). Around the time of reach movement onset, responses of V6A neurons cannot be fully explained by a gaze-centered reference frame and an eye position gain field, suggesting that some V6A neurons use a nonretinocentric frame of reference (15).

SI Methods

All procedures conformed to the Guide for the Care and Use of Laboratory Animals and were approved by the Washington University Institutional Animal Care and Use Committee.

General Recording Procedures. Eye position was monitored by the scleral search coil technique (CNC Engineering). Hand position was monitored by a 13.2 × 13.2-cm custom-built touch panel that uses finely spaced (3 mm) horizontal and vertical infrared beams 1–3 mm above a smooth-touch surface (2-ms temporal resolution). The touch screen was mounted such that the center was approximately aligned with the line of sight when the eyes were estimated to be in primary position. The screen center then formed the origin of our coordinate system for measuring eye and hand position. All measurements are, therefore, in screen coordinates (i.e., the location at which eyes intercept the screen and the location at which the animal touches the screen). As shorthand, we refer to these measurements throughout the text as eye and hand position, respectively. We define a hand-centered representation of a target position as the location of the target in a coordinate system whose origin coincides with the location of the hand, or equivalently, a vector extending from the location of the hand to the location of the target.

The animals sat in a custom-designed monkey chair (Crist Instrument) with a fully open front to provide unimpaired reaching movements. Visual stimuli were back-projected by a CRT (cathode ray tube) projector onto the touch surface, which was mounted vertically about 25 cm in front of the animal. The recording room was sound-attenuating and lightproof, such that a dark-adapted human could detect no light when the projector was turned on but projecting no targets. Extracellular recordings were made using glass-coated tungsten electrodes (Alpha Omega). We recorded neuronal activity in PRR and identified 259 well-isolated, stable cells that showed spatial tuning. Cells were recorded from the right hemisphere from monkey G (n = 102) and left hemisphere from monkey S (n = 157), with each animal reaching using its contralateral limb. To guide the placement of our recording tracks and localize recording sites, we acquired high-resolution MRI of the monkeys' brains with an MR lucent "phantom" in the recording chamber using methods described elsewhere (16–18). We then created custom MRI atlases for each animal and used those atlases to aim electrodes at the posterior end of the medial bank of the IPS. Based on the MRI-mediated maps, electrodes were lowered, aiming at locations along the medial bank of IPS (~90% of tracks). Localization was accurate to within 1 mm, as determined by injecting and then visualizing MR-lucent manganese in the brain in several sessions.

Behavioral Tasks. The number of targets, spacing, and eccentricity were established using a series of simulations. We simulated neuronal responses to a variety of task designs using idealized cells whose characteristics (tuning width, response variability, etc.) were based on cells that we recorded from PRR in previous studies (16, 17, 19). We varied the task parameters, used our idealized cells to generate artificial data, and then, analyzed those data to optimize the task design and ensure that the fitting procedure was reliable.

We recorded neurons from two monkeys (*Macaca mulatta*) during a visually guided delayed reaching task. These data were also used for a previous report (20). We first mapped each neuron's preferred direction (Fig. S1*B*). Obtaining a full tuning curve, including the peak neuronal response, is critical for distinguishing reference frame effects from gain field effects (7). For our main task (Fig. 1*B*), we centered an array of five targets on each cell's preferred direction.

In the preferred direction mapping task, animals made center-out arm movements while maintaining central fixation (19). Animals first fixated and pointed at a blue center target (2.4° × 2.4° within a 4° radius). A peripheral target (2.4° × 2.4°) appeared at 1 of 16 locations at 12–14° eccentricity. After a variable delay (800–1,200 ms), the center target shrank to a single pixel (0.3° × 0.3°), signaling the animal to reach to the peripheral target without breaking eye fixation. The preferred direction (i.e., the direction associated with the peak neuronal response) (Fig. S1*B*) determined the target placement for the main task. Capturing the peak response is critical for distinguishing reference frame effects from gain field effects (7). Our method worked well: 91% of the cells with at least 5 sp/s of spike-variance explained showed peak firing at one of three central target locations (*T2*–*T4*).

In the main task (Fig. 1*B*), an initial eye target and an initial hand target, each 0.9° × 0.9°, were each presented at one of three possible locations (*P1*–*P3*). Monkeys fixated the initial eye target and touched the initial hand target. One or both of the two initial targets were always at the center of the screen, directly in front of the animal (*P2*). The other two possible targets (*P1* and *P3*) were located 7.5° to either side of *P2* along an imaginary line through the center of the screen and perpendicular to the cell's preferred direction, as determined in the preferred direction mapping task. Five different configurations of the starting eye and hand position were used (see box in Fig. 1*B*). Four hundred and fifty ms after the animal touched and fixated the initial hand and eye targets, a peripheral target for a final reach (2.4° × 2.4°) appeared at one of eight possible target locations. These peripheral targets lay in or near the receptive field (*T1*–*T5* in Fig. 1*B*; spaced 7.5° apart), lying on a line perpendicular to the preferred direction and 12–14° away from the center target (*P2* to *T3*). There was also one target opposite to the preferred direction and two targets orthogonal to the preferred direction, but data from these targets were not analyzed (*T6*, *T7*, and *T8*). On each trial, animals maintained the initial eye and hand position within 4° and 5°, respectively, for a variable delay period (900–1,300 ms) after the peripheral target onset. The initial eye and hand targets then shrank to a single pixel, cueing the animal to reach out and touch within 5–6° of the peripheral target without moving the eyes from the initial eye target. A median and mode of 8 ± 1.11 repetitions (± SD) were collected for each of the 40 unique trial types from each cell in the main task (Fig. 1*B*). When an error occurred (a failure to achieve or maintain fixation or touch at the initial targets throughout the delay period, inaccurate reach to the peripheral target, or failure to maintain fixation during the reach), the trial was aborted, a multicolored square appeared briefly on the screen as a familiar error signal, and a short (0.5–1.5 s) timeout ensued. Aborted trials were excluded from further analyses. Successful trials were rewarded with a drop of water or juice. Results and Table S1 show reaction times and success rates of individual monkeys.

Details on Model Parameters. The full model (Eq. **1**) inputs were firing rates, target eccentricity along the preferred direction (*ecc*; the distance between *P2* and *T3* in Fig. 1*B* measured in degrees of visual angle), target displacement in a direction perpendicular to the preferred direction (*T*; degrees of visual angle measured along the line connecting *T1* to *T5*), and displacement of the initial eye (*E*) and hand target (*H*) from the center point (*P2*) in degrees of visual angle. We use the terms gaze or eye position and hand position to define the location on the screen at which we measured eye and hand positions (i.e., fixation and pointing positions in 2D screen coordinates). The output parameters were baseline (*k*) and peak amplitude of modulation (*pa*), both in spikes per second, offset of the center of the tuning curve from the central target (*T3*) in degrees of visual angle (*mid*), standard deviation (*sd*) of the Gaussian curve in degrees of visual angle, the amplitudes of the eye-position gain field (g_{Eye}) and the hand-position gain field (g_{Hand}), both in fractional modulation per degree, and a unitless weight parameter (*weight*). The *weight* parameter described the frame of reference for each cell with

weights of 1 and 0 corresponding to pure gaze- and hand-centered cells, respectively. During the fitting procedure, parameters were constrained as follows: from −5 to 100 sp/s for *k*, from 0 to 300 sp/s for *pa*, from −1.5 to 2.5 for *weight*, from −0.15 to 0.15 (−15% to 15%) of modulation per degree for g_{Eye}, g_{Hand}, and g_{Diff}, from −45 to 45° for *mid*, and from 15 to 60° for *sd*. These constraints were based on previously recorded data and inspection of model fits.

Location of PRR. PRR cells straddle the boundary between the medial intraparietal area (MIP) and V6A in posterior parietal cortex (PPC). PRR was first identified as a region with a high proportion of neurons with strong visual responses and memory activity for visually presented targets that is much stronger on impending reach trials than on impending saccade trials (19). This region lies on the posterior portion of the medial bank of the IPS, close to the junction with the parieto-occipital sulcus (POS), and may extend onto the lateral bank (Fig. 1*D* and Fig. S1*A*) (16, 17, 19). By combining our functional definition of PRR with published histological tract tracing data, it can be seen that PRR primarily overlaps the anterior portion of V6A, the posterior portion of MIP, and a small part of LOP/cIPS (Fig. 1*D* and Fig. S1*A*). Although the borders of these anatomically defined areas vary somewhat from animal to animal and can vary greatly from study to study (21), it is clear that PRR is well separated from LIP and from the portion of the medial bank that lies directly across from LIP.

1. Pesaran B, Nelson MJ, Andersen RA (2006) Dorsal premotor neurons encode the relative position of the hand, eye, and goal during reach planning. *Neuron* 51: 125–134.
2. Batista AP, Buneo CA, Snyder LH, Andersen RA (1999) Reach plans in eye-centered coordinates. *Science* 285:257–260.
3. Mullette-Gillman OA, Cohen YE, Groh JM (2005) Eye-centered, head-centered, and complex coding of visual and auditory targets in the intraparietal sulcus. *J Neurophysiol* 94:2331–2352.
4. Batista AP, et al. (2007) Reference frames for reach planning in macaque dorsal premotor cortex. *J Neurophysiol* 98:966–983.
5. Buneo CA, Batista AP, Jarvis MR, Andersen RA (2008) Time-invariant reference frames for parietal reach activity. *Exp Brain Res* 188:77–89.
6. Stricanne B, Andersen RA, Mazzoni P (1996) Eye-centered, head-centered, and intermediate coding of remembered sound locations in area LIP. *J Neurophysiol* 76: 2071–2076.
7. Mullette-Gillman OA, Cohen YE, Groh JM (2009) Motor-related signals in the intraparietal cortex encode locations in a hybrid, rather than eye-centered reference frame. *Cereb Cortex* 19:1761–1775.
8. Jay MF, Sparks DL (1984) Auditory receptive fields in primate superior colliculus shift with changes in eye position. *Nature* 309:345–347.
9. Jay MF, Sparks DL (1987) Sensorimotor integration in the primate superior colliculus. II. Coordinates of auditory signals. *J Neurophysiol* 57:35–55.
10. Metzger RR, Mullette-Gillman OA, Underhill AM, Cohen YE, Groh JM (2004) Auditory saccades from different eye positions in the monkey: Implications for coordinate transformations. *J Neurophysiol* 92:2622–2627.
11. Avillac M, Denève S, Olivier E, Pouget A, Duhamel JR (2005) Reference frames for representing visual and tactile locations in parietal cortex. *Nat Neurosci* 8:941–949.
12. Fetsch CR, Wang S, Gu Y, Deangelis GC, Angelaki DE (2007) Spatial reference frames of visual, vestibular, and multimodal heading signals in the dorsal subdivision of the medial superior temporal area. *J Neurosci* 27:700–712.
13. Caminiti R, Johnson PB, Galli C, Ferraina S, Burnod Y (1991) Making arm movements within different parts of space: The premotor and motor cortical representation of a coordinate system for reaching to visual targets. *J Neurosci* 11:1182–1197.
14. Kalaska JF, Scott SH, Cisek P, Sergio LE (1997) Cortical control of reaching movements. *Curr Opin Neurobiol* 7:849–859.
15. Marzocchi N, Breveglieri R, Galletti C, Fattori P (2008) Reaching activity in parietal area V6A of macaque: Eye influence on arm activity or retinocentric coding of reaching movements? *Eur J Neurosci* 27:775–789.
16. Calton JL, Dickinson AR, Snyder LH (2002) Non-spatial, motor-specific activation in posterior parietal cortex. *Nat Neurosci* 5:580–588.
17. Chang SW, Dickinson AR, Snyder LH (2008) Limb-specific representation for reaching in the posterior parietal cortex. *J Neurosci* 28:6128–6140.
18. Kalwani RM, Bloy L, Elliott MA, Gold JI (2009) A method for localizing microelectrode trajectories in the macaque brain using MRI. *J Neurosci Methods* 176:104–111.
19. Snyder LH, Batista AP, Andersen RA (1997) Coding of intention in the posterior parietal cortex. *Nature* 386:167–170.
20. Chang SW, Papadimitriou C, Snyder LH (2009) Using a compound gain field to compute a reach plan. *Neuron* 64:744–755.
21. Lewis JW, Van Essen DC (2000) Mapping of architectonic subdivisions in the macaque monkey, with emphasis on parieto-occipital cortex. *J Comp Neurol* 428:79–111.

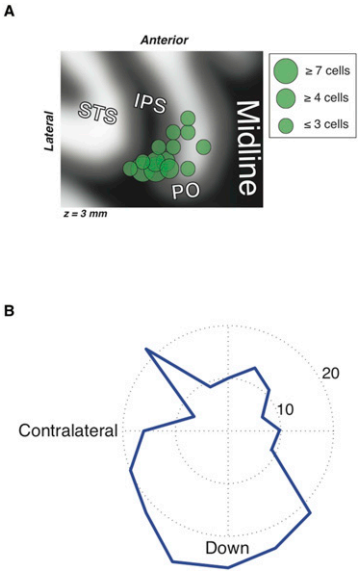

Fig. S1. (*A*) Recording sites from animal S projected on a horizontal slice (3 mm from the surface) obtained from MR imaging. (*B*) Distributions of preferred directions in polar coordinates for all cells (n = 259). Preferred directions are adjusted so that the right side of the plot corresponds to the contralateral visual hemifield for both monkeys. Downward and contralateral directions are more strongly represented.

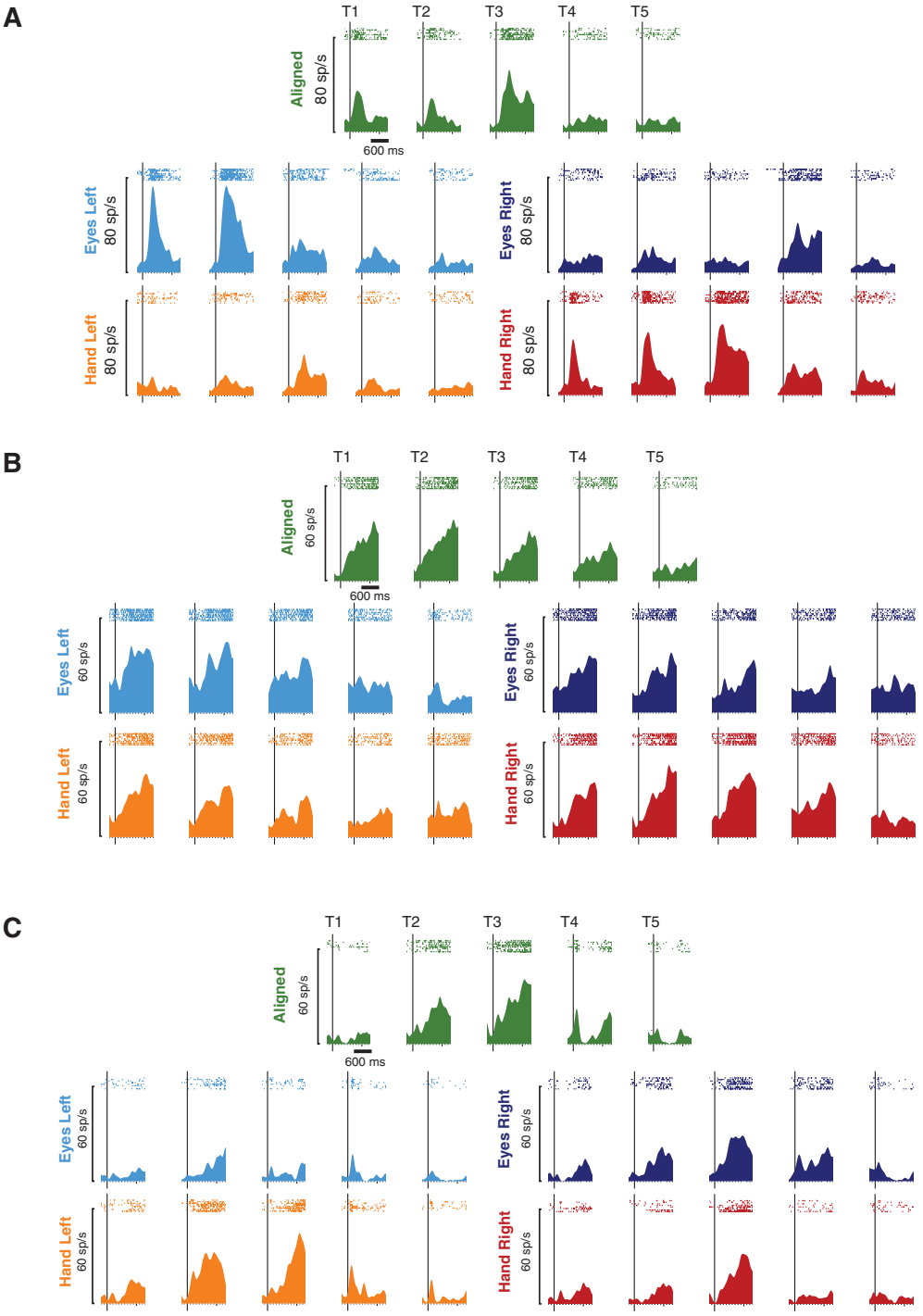

Fig. S2. Activity of example neurons (Fig. 2) aligned on target onset. (*A*) Activity of the same example cell shown in Fig. 2*A* that uses a gaze-centered frame of reference. (*B*) Activity of the same example cell shown in Fig. 2*B* that uses a hand-centered frame of reference is shown aligned on target onset. (*C*) Activity of the same example cell shown in Fig. 2*C* that uses an intermediate coding is shown aligned on target onset. The format is the same as in Fig. 2.

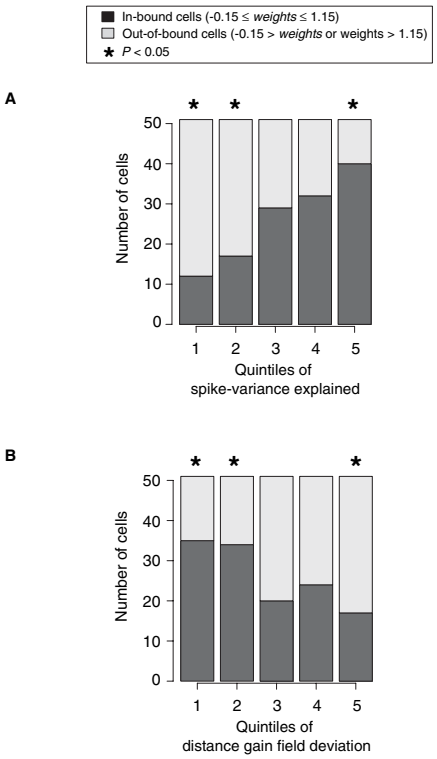

Fig. S3. Separation of in-bound and out-of-bound cells. (*A*) The 255 cells for which the model converged were divided into ascending quintiles based on spike-variance explained (least to most). The fractions of in-bound (dark bars) and out-of-bound cells (light bars) in each quintile are indicated. In-bound cells were overrepresented in the upper quintiles (i.e., higher spike-variance explained), whereas out-of-bound cells were overrepresented in the lower quintiles. (*B*) A similar analysis applied to distance gain field deviations. Cells were divided into ascending quintiles based on the mismatch between eye and hand gain field amplitudes. In-bound cells were overrepresented in the lower quintiles (i.e., less deviation and therefore, a better match of the two gain fields), whereas out-of-bound cells were overrepresented in the upper quintiles (more deviation and poorer match). *$P < 0.05$ by proportion test.

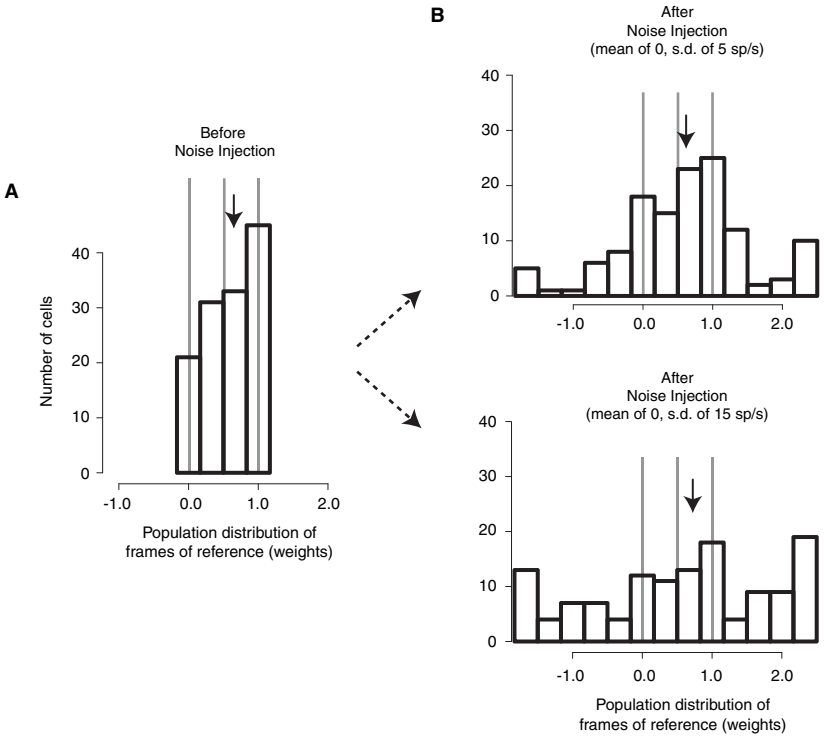

Fig. S4. Effects of noise injection on in-bound cells. (*A*) Distribution of reference frame values (weights from Eq. **1**) for all in-bound cells ($n = 130$) before noise injection. (*B*) Reference frame distributions after injecting Gaussian noise with SD of 5 sp/s (*Upper*) or 15 sp/s (*Lower*). Three vertical lines represent values corresponding to a pure hand-centered weight (0), a pure gaze-centered weight (1), and a representation halfway in between the two (0.5). The arrow indicates the median of the distribution.

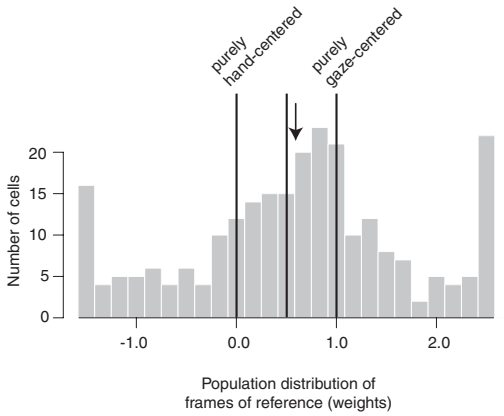

Fig. S5. The distribution of reference frame weights from the delay period is shown for all cells that converged to the full model (Eq. **1**) (n = 255 of 259 cells). The three vertical lines represent values corresponding to a pure hand-centered representation (weight = 0), a pure gaze-centered representation (weight = 1), and a representation halfway in between the two (weight = 0.5). The arrow indicates the median of the distribution.

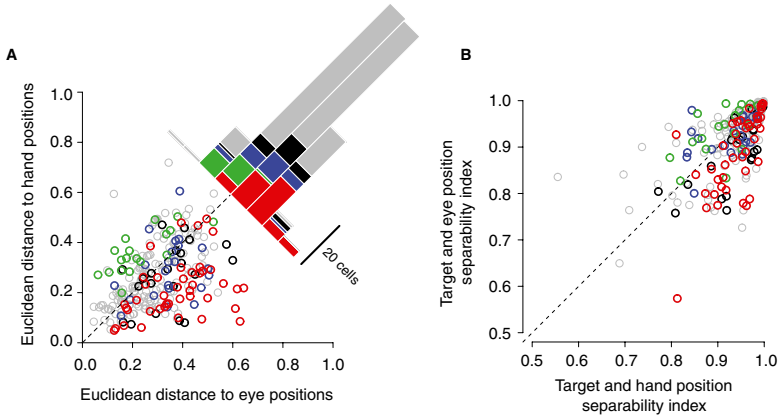

Fig. S6. Additional reference frame analyses. Data from all 259 cells are shown in each panel. Cells with a spike-variance explained of at least 5 sp/s are shown in color: red for gaze-centered cells, green for hand-centered cells, blue for intermediate cells, and black for indeterminate cells based on stepwise regression. Cells with spike-variance explained of less than 5 sp/s are gray. (*A*) Tuning shift analysis based on the Euclidean distance method. Euclidean distances for different starting eye positions and hand positions are plotted. (*B*) Tuning shift analysis using the singular value decomposition method. The separability indices are plotted for target and eye positions against target and hand positions.

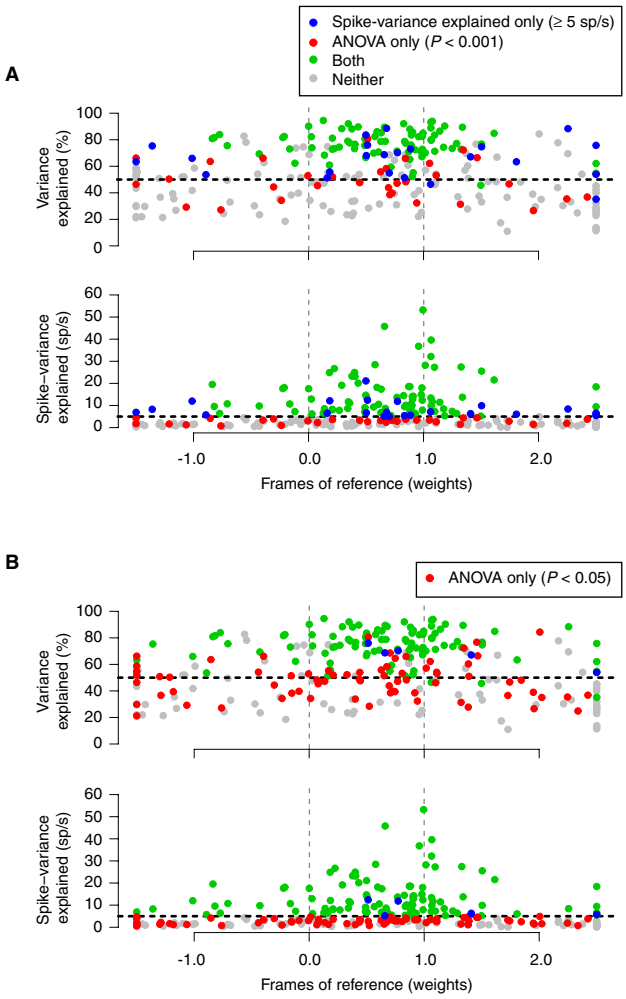

Fig. S7. Comparison of variance explained, spike-variance explained, and ANOVA. (*A*) Variance explained (r^2) and spike-variance explained are plotted as a function of reference frame (weight parameter from Eq. **1**). Color coding indicates selection by ANOVA ($P < 0.001$; red), spike-variance explained (a stepwise regression performed on the full model; Eq. **1**; blue), or both (green). The dotted horizontal lines in *Upper* and *Lower* indicate a variance explained of 50% and spike-variance explained of 5 sp/s, respectively. (*B*) Similar plots comparing cells selected but using a less strict ANOVA criterion ($P < 0.05$). Same format as in *A*.

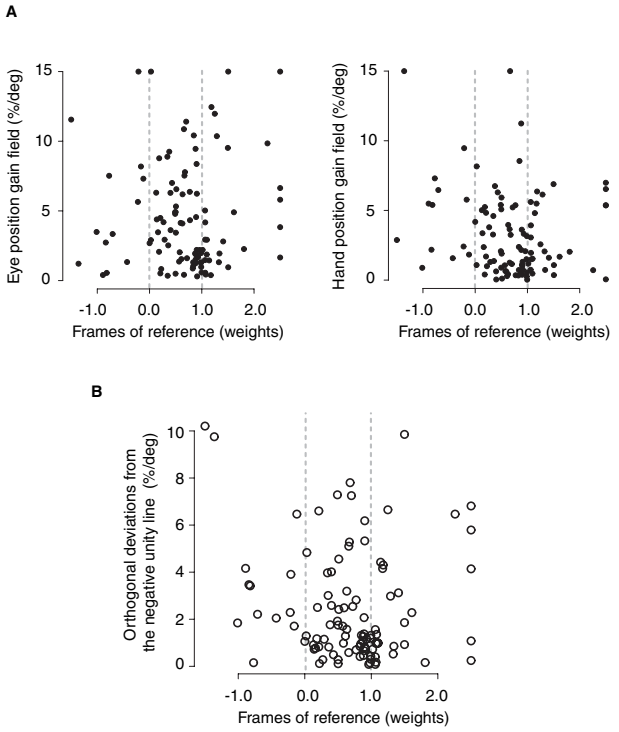

Fig. S8. Relationships between reference frames and the individual eye and hand gain fields. (*A*) Absolute eye position gain fields (*Left*) and hand position gain fields (*Right*; percent per degree) are plotted as a function of the reference frame (weight) (Eq. **1**). Vertical dotted lines indicate a pure hand-centered and pure gaze-centered weight. (*B*) The absolute orthogonal distances of each data point from the negative unity line from Fig. 4 (i.e., the degree of mismatch in the compound gain field) is plotted as a function of the reference frame for that cell (weights) (Eq. **1**). Vertical dotted lines at $x = 0$ and $x = 1$ indicate pure hand-centered and gaze-centered weights, respectively.

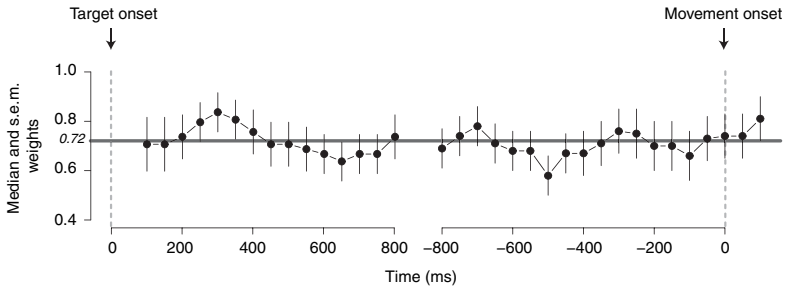

Fig. S9. Temporal evolution of reference frames. Median weights and SEM (from the full model) are plotted over the course of the task. Data points were obtained from a 200-ms sliding window with a 50-ms step size. The first data point shown corresponds to the data from 0 to 200 ms from target onset. The median of our population based on a larger interval (Fig. 3*A*) is indicated by the solid line across the plot.

Table S1. Behavioral performance

	Absolute starting eye position error (deg; median ± SD)		Absolute starting hand position error		Absolute final hand position error	
Monkey ID	Horizontal	Vertical	Horizontal	Vertical	Horizontal	Vertical
G	0.90 ± 0.88	1.19 ± 1.05	2.35 ± 2.09	1.80 ± 1.60	2.40 ± 2.31	2.11 ± 2.08
S	0.60 ± 0.55	0.74 ± 0.65	1.85 ± 1.79	1.34 ± 1.10	2.05 ± 1.92	1.30 ± 1.26

Median absolute distance of eye and hand landing positions from the starting eye, hand, and final hand positions.